Proceedings of the ASME 2010 3rd Joint US-European Fluids Engineering Summer Meeting and 8th International Conference on Nanochannels, Microchannels, and Minichannels
FEDSM-ICNMM2010
August 1-5, 2010, Montreal, Canada

FEDSM-ICNMM2010-31156

HERMITE-DG METHOD FOR PDF-EQUATIONS MODELLING DISPERSIONS IN TURBULENT BOUNDARY LAYERS INCLUDING STREAMWISE VELOCITY.

Peter J. van Dijk*
School of Mechanical and Systems Engineering
Newcastle University
Newcastle upon Tyne, NE1 7RU, UK
Email: pjvd00@gmail.com

David C. Swailes
School of Mechanical and Systems Engineering
Newcastle University
Newcastle upon Tyne, NE1 7RU, UK
Email: d.c.swailes@ncl.ac.uk

ABSTRACT

A novel methodology is presented for the numerical treatment of multi-dimensional pdf (probability density function) models used to study particle transport in turbulent boundary layers. A system of coupled Fokker-Planck type equations is constructed to describe the transport of phase-space conditioned moments of particle and fluid velocities, both streamwise and wall-normal. Unlike conventional moment-based transport equations this system allows for an exact treatment of particle deposition at the flow boundary. Moreover, the equations in the system are linear and can be solved in a sequential fashion; there is no closure problem to address.

A Hermite-Discontinuous Galerkin scheme is employed to treat the system. The choice of Hermite basis functions in combination with an iterative rescaling approach, allows for efficient discretization of the, effectively, 5-dimensional phase-space domain. Results demonstrate the effectiveness of the methodology in resolving distributions near an absorbing boundary.

INTRODUCTION

The formulation of probability density function (pdf) models to describe the transport of dispersed particles in turbulent flow is well established, and such models have provided valuable insights in the study of this type of multiphase flow. In this context a pdf model refers to a differential equation for an ensemble-average pdf that defines the joint distribution of various particle variables. Two distinct but closely related types of pdf models have been developed in recent years; these can be classified as particle-pdf equations and particle-fluid-pdf equations. The modern development of particle-pdf equations is largely attributable to the work of Reeks [1], extending the earlier work of Buyevich [2]. In its basic form this approach considers the joint distribution of particle position $\mathbf{x_p}(\mathbf{t})$ and velocity $\mathbf{v_p}(\mathbf{t})$ and constructs an equation for the corresponding pdf $p(\mathbf{x}, \mathbf{v}, \mathbf{t})$.

The development of particle-fluid-pdf equations, sometimes referred to as generalized Langevin models, is due primarily to the work of Simonin and Minier [3], and builds on Lagrangian models for turbulence. In the particle-fluid approach the local fluid velocity $\mathbf{u_p}(\mathbf{t})$ experienced by a particle is treated as an additional variable, and the particle-fluid-pdf equation determines the corresponding pdf $\phi(\mathbf{x}, \mathbf{v}, \mathbf{u}, \mathbf{t})$.

While there is a significant body of work concerned with the formulation of both particle- and particle-fluid-pdf equations there are, in contrast, very few studies concerned with the direct numerical treatment of these pdf models. The most evident reason for this is the high dimensionality of the phase-space that requires discretization. Consequently, in the application of pdf models it has become common practice to reduce these to systems of mass, momentum and stress type transport equations involving moments of the phase-space variables. However, this reduction comes at a price; the resulting systems are nonlinear, and require closure. Further, in general it is not possible to translate particle-surface interactions into exact boundary conditions for the moments. All this is in marked contrast to the pdf models,

*Address all correspondence to this author.

which are essentially linear and closed, and which can accommodate complex particle-surface interactions in a natural and exact way. Therefore, notwithstanding the challenge imposed by high phase-space dimensionality, there is a need for efficient numerical methods that can treat pdf models applied to regimes where particle-surface interactions are critical, and where moment closure modelling is difficult. The most obvious of such regimes are turbulent boundary layers.

Previous work on the numerical treatment of pdf models in turbulent boundary layers has, to the authors' knowledge, focused exclusively on particle pdf equations [4, 5].

The application of the particle-fluid pdf model to turbulent boundary layers is outlined in the next section. Next, an important innovation is introduced that permits a reduction of the phase-space dimensionality of the pdf model. This results is a system of Fokker-Planck type pdf equations which preserve, despite the reduced dimensionality, essential information about both stream-wise and wall-normal features of the underlying pdf. The numerical treatment of this system of Fokker-Planck equations is considered in the subsequent section where a Hermite-Discontinuous Galerkin (H-DG) numerical approach is developed.

PARTICLE-FLUID PDF MODEL FOR TURBULENT BOUNDARY LAYERS

As noted already, pdf models are particularly well suited to the study of particle transport in boundary layer flows since these models allow non-trivial particle-surface interactions to be accurately formulated as pdf equation boundary conditions. Particle deposition (adhesion) at a flow boundary is not only a commonly occurring and important case but also, from a numerical perspective, one of the most challenging since it can result in the presence of large gradients within particle velocity distributions. It is this type of particle-surface interaction that is considered here.

Attention is restricted to simple versions of the particle-fluid pdf model. In particular, only those forms relevant to dilute systems are considered. Consequently no consideration is given to turbulence attenuation (two-way coupling) or particle-particle interactions. Further, only models relating to mono-disperse systems are considered and, allied to this, it is assumed that the trajectory $\boldsymbol{x}_p(t)$ of an individual particle can be described by a simple equation of motion (Stokes drag)

$$\ddot{\boldsymbol{x}}_p = \dot{\boldsymbol{v}}_p = \beta\big(\mathbf{U}(\mathbf{x_p}, \mathbf{t}) - \mathbf{v_p}\big) + \boldsymbol{g}, \tag{1}$$

where $\beta = 6\pi\mu a/m$ represents the particle relaxation rate with μ the fluid viscosity, a the particle radius, and m the particle mass. $\mathbf{U}(\mathbf{x}, \mathbf{t})$ denotes the underlying fluid velocity field. Although simple, equation Eqn. (1) does represent an important and commonly used model for particle motion in gas-solid flows, and so the corresponding pdf models are of considerable utility.

The formulation of particle-fluid pdf equations proceeds by modelling the normalized fluctuating fluid velocity along particle trajectories. Decompose the fluid velocity $\boldsymbol{U}$ into mean and fluctuating components, $\boldsymbol{U} = \langle \boldsymbol{U} \rangle + \boldsymbol{U}'$, and then write $\mathbf{u}(\boldsymbol{x}, \mathbf{t}) = \boldsymbol{Q}(\boldsymbol{x}) \cdot \boldsymbol{U}'(\boldsymbol{x}, \mathbf{t})$ where $\boldsymbol{Q} = \mathrm{diag}(\sigma_1^{-1}, \sigma_2^{-1})$ represents the velocity normalization matrix, where the characteristic velocity scalings $\sigma_i = \sigma_i(\boldsymbol{x})$ are defined in terms of the turbulent fluid stresses, $\sigma_i^2 = \langle U_i' U_i' \rangle$. The normalised fluctuating fluid velocity along a particle trajectory, $\mathbf{u_p}(\mathbf{t}) = \boldsymbol{u}(\boldsymbol{x}_\mathbf{p}, \mathbf{t})$, is then modelled via a stochastic differential equation of the form, see e.g. [6],

$$\dot{\boldsymbol{u}}_p = \boldsymbol{\mathcal{G}}(\boldsymbol{x}_p, \boldsymbol{u}_p) + \boldsymbol{\Gamma}, \tag{2}$$

where $\boldsymbol{\Gamma}$ is zero-mean Gaussian stochastic field, having second-order moments

$$\langle \boldsymbol{\Gamma}(\boldsymbol{x}, t) \boldsymbol{\Gamma}(\boldsymbol{x}, t') \rangle = \delta(t - t') \boldsymbol{\Sigma}(\boldsymbol{x}). \tag{3}$$

The rate matrix $\boldsymbol{\alpha}$ is of the form $\alpha(\boldsymbol{x}) = \mathrm{diag}(\tau_1^{-1}, \tau_2^{-1})$, with the $\tau_i(\boldsymbol{x})$ representing decorrelation time scales for the components of $\mathbf{u_p}$. Following [7], $\boldsymbol{\Sigma}(\boldsymbol{x}_p)$ is specified by

$$\boldsymbol{\Sigma} = \boldsymbol{\alpha} \cdot \langle \boldsymbol{u}\boldsymbol{u} \rangle + \langle \boldsymbol{u}\boldsymbol{u} \rangle \cdot \boldsymbol{\alpha}^\top. \tag{4}$$

The term $\boldsymbol{\mathcal{G}}$ consists of a response term and a correction term to prevent spurious drift, see [8]. Also following [7] it is given by

$$\boldsymbol{\mathcal{G}}(\boldsymbol{x}, \boldsymbol{u}) = -\boldsymbol{\alpha}(\boldsymbol{x}) \cdot \boldsymbol{u} + \nabla \cdot \langle \boldsymbol{U}' \boldsymbol{u} \rangle. \tag{5}$$

Then the pdf $\Phi(\boldsymbol{x}, \boldsymbol{v}, \boldsymbol{u}, t)$, defining the joint distribution of $\boldsymbol{x}_p, \boldsymbol{v}_p, \boldsymbol{u}_p$ as determined by Eqn. (1), Eqn. (2), takes the form of a Fokker-Planck equation [9]

$$\frac{\partial}{\partial t}\Phi + \frac{\partial}{\partial \boldsymbol{x}} \cdot \Phi \boldsymbol{v} + \frac{\partial}{\partial \boldsymbol{v}} \cdot \boldsymbol{\mathcal{F}}\Phi + \frac{\partial}{\partial \boldsymbol{u}} \cdot \boldsymbol{\mathcal{G}}\Phi = \boldsymbol{\mathcal{D}} : \frac{\partial^2}{\partial \boldsymbol{u}^2}\Phi, \tag{6}$$

where $\boldsymbol{\mathcal{F}} = \beta\left(\langle \boldsymbol{U} \rangle + \boldsymbol{Q}^{-1} \cdot \boldsymbol{u} - \boldsymbol{v} + \boldsymbol{v}_g\right)$ and $\boldsymbol{\mathcal{D}} = \frac{1}{2}\boldsymbol{\Sigma}$. The gravitational settling velocity is represented by $\boldsymbol{v}_g = g/\beta$.

The general flow configuration is depicted in Fig. 1. Attention is restricted to stationary and x_1 invariant solutions to Eqn. (6). The flow is considered to be statistically stationary, with the streamwise directed mean fluid flow velocity $\langle \boldsymbol{U} \rangle = (\langle U_1 \rangle, 0)$, the fluid Reynolds stresses $\langle \boldsymbol{U}'\boldsymbol{U}' \rangle$, and integral time scales for the fluid τ_i all treated as only x_2 dependent. The boundary layer profiles of these flow statistics, which are inputs into the model given by Eqn. (6), have been constructed

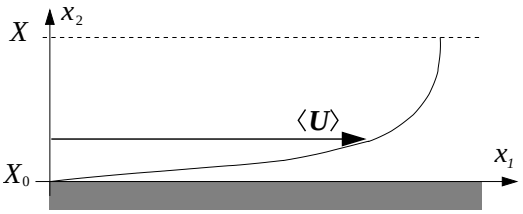

FIGURE 1. BOUNDARY LAYER CONFIGURATION.

from fits to the DNS data of [10]. The fluid time scales are taken from [11].

Particles in this boundary layer flow that strike the surface at $x_2 = X_0$ stick and, consequently, there is no reflux of particles from this surface. This translates into the following boundary condition for Eqn. (6) at X_0,

$$\Phi = 0, \quad \text{for } v_2 > 0, \text{all } v_1, u_1, u_2. \tag{7}$$

The location of X_0 is interpreted as the point that is one particle radius away from the wall (at $x_2 = 0$). In wall units this particle radius is given by $X_0 = \sqrt{\frac{9}{2}\beta^{-1}\rho_f/\rho_p}$, where ρ_f, ρ_p represent the material densities of, respectively, the fluid and the particles.

It is also necessary to attach a boundary condition to Eqn. (6) at $x_2 = X$, which represents some prescribed interface between the turbulent core and the near wall region in which the pdf model is applied. With the bulk flow treated as a source for the particles entering the domain $X_0 < x_2 < X$ the interface condition at $x_2 = X$ will be of the form

$$\Phi = \Phi_X(\boldsymbol{v}, \boldsymbol{u}), \quad \text{for } v_2 < 0, \text{all } v_1, u_1, u_2\ , \tag{8}$$

where Φ_X represents the joint particle-fluid velocity distribution that is characteristic of the bulk flow. Appropriate models for this distribution can be derived by assuming it to be both temporally and spatially invariant. Then, from the corresponding form of Eqn. (6), the Gaussian distribution is obtained for $\Phi_{\rm X}(\boldsymbol{v}, \boldsymbol{u})$. This Gaussian is expressed in terms of the phase-space variable $\boldsymbol{z} = (\boldsymbol{v}, \boldsymbol{u})$, and is centered on the associated mean $\widehat{\boldsymbol{z}} = (\langle \boldsymbol{U} \rangle(X) + \boldsymbol{v}_g, \boldsymbol{0})$. Expressions for the elements of the covariance matrix $\boldsymbol{\Theta}$, which describes correlations in the fluctuating particle and fluid velocities in the bulk flow are presented in block form as

$$\boldsymbol{\Theta}_{11} = \begin{bmatrix} \eta_1\sigma_1^2 & \overline{\eta}\sigma_1\sigma_2 r \\ \overline{\eta}\sigma_1\sigma_2 r & \eta_2\sigma_2^2 \end{bmatrix}_X, \qquad \boldsymbol{\Theta}_{22} = \begin{bmatrix} 1 & r \\ r & 1 \end{bmatrix}_X, \tag{9}$$

$$\boldsymbol{\Theta}_{12} = \boldsymbol{\Theta}_{21}^\top = \begin{bmatrix} \eta_1\sigma_1 & \eta_2\sigma_1 r \\ \eta_1\sigma_2 r & \eta_2\sigma_2 \end{bmatrix}_X \tag{10}$$

where $\eta_i = (1 + S_i)^{-1}$, $\overline{\eta} = \frac{1}{2}(\eta_1 + \eta_2)$, with $S_i = (\beta\tau_i)^{-1}$ the particle Stokes number associated with the fluid time scale τ_i, and $r = \langle U_1' U_2' \rangle / \sigma_1\sigma_2$ is the fluid correlation coefficient.

TREATMENT OF THE STREAMWISE VELOCITY DIMENSIONS

The domain of Φ, however, is still a five-dimensional phase-space and, from a computational perspective, this poses a serious limitation on the numerical resolution that can be realised from a discretization of this form of the model. Previous work has considered a further reduction of phase-space dimensions by restricting attention to the wall normal velocity variables, v_2 and u_2: By integrating equation (6) over v_1 and u_1 a model is obtained for the marginal pdf $\phi = \iint \Phi dv_1 du_1$. However, while this approach provides a reduced model that still allows for exact modelling of particle absorption, it is clear that the level of information obtainable from the model is limited. In particular it provides no information about the streamwise features of the original pdf Φ. To overcome this an extension of the approach is proposed which includes, in addition to the marginal pdf ϕ, the following marginal moments of Φ

$$\Upsilon^{n,m}(x_2, v_2, u_2) = \iint v_1^n u_1^m \Phi(x_2, \boldsymbol{v}, \boldsymbol{u}) dv_1 du_1\ . \tag{11}$$

Note that $\Upsilon^{0,0} = \phi(x_2, v_2, u_2)$. The higher-order moments, $(n, m) \neq (0, 0)$, provide information about streamwise particle-fluid velocity moments. Specifically

$$\Upsilon^{n,m}(x_2, v_2, u_2) = \phi\overline{\overline{v_1^n u_1^m}} \tag{12}$$

where $\overline{\overline{\cdot}}$ denotes a phase-space conditioned average:

$$\overline{\overline{f(\boldsymbol{x}, \boldsymbol{v}, \boldsymbol{u})}}(x_2, v_2, u_2) = \langle f(\boldsymbol{x}_p(t), \boldsymbol{v}_p(t), \boldsymbol{u}_p(t)) \rangle_s\ . \tag{13}$$

The subensemble $\langle \cdot \rangle_s$ is over those phase-space trajectories $(\boldsymbol{x}_p, \boldsymbol{v}_p, \boldsymbol{u}_p)$ for which $x_2(t) = x_2$, $v_2(t) = v_2$, and $u_2(t) = u_2$. The more familiar spatially conditioned averages, giving the mean-field values of the particle-fluid variables, are related to the phase-space conditioned averages $\Upsilon^{n,m}$ by

$$\overline{v_1^{n_1} u_1^{m_1} v_2^{n_2} u_2^{m_2}}(x_2) = \frac{1}{\rho} \iint v_2^{n_2} u_2^{m_2} \Upsilon^{n_1, m_1} dv_2 du_2\ , \tag{14}$$

where $\rho(x_2) = \iint \phi dv_2 u_2$ denotes the particle number density.

Transport equations for the $\Upsilon^{n,m}$ follow easily from (6) and have the general form,

$$\frac{\partial}{\partial x_2} v_2 \Upsilon^{n,m} + \frac{\partial}{\partial v_2} \mathcal{F}_2 \Upsilon^{n,m} + \frac{\partial}{\partial u_2} \mathcal{G}_2 \Upsilon^{n,m} = \mathcal{D}_{22} \frac{\partial^2}{\partial {u_2}^2} \Upsilon^{n,m} + S^{n,m}. \quad (15)$$

Equation (15) is a Fokker-Planck equation for $\Upsilon^{n,m}$ with an additional source term $S^{n,m}$. This has the form

$$\begin{aligned} S^{n,m} &= n(\beta\langle U\rangle + g_1)\Upsilon^{n-1,m} + n\beta\sigma_1 \Upsilon^{n-1,m+1} \\ &+ m(m-1)\mathcal{D}_{11}\Upsilon^{n,m-2} + m\frac{d\langle U_2' u_1\rangle}{dx}\Upsilon^{n,m-1} \\ &- 2m\mathcal{D}_{12}\frac{\partial}{\partial u}\Upsilon^{n,m-1} - (n\beta + m\alpha_1)\Upsilon^{n,m}\,. \end{aligned} \quad (16)$$

Several crucial points are of note with regard to the system of equations given by Eqn. (15) and Eqn. (16). Firstly, exact boundary conditions for all of the $\Upsilon^{n,m}$ can be constructed. This follows immediately from the definition of the $\Upsilon^{n,m}$ and the fact that Φ is specified (for $v_2 \gtrless 0$) at the domain boundaries. Secondly, Eqn. (15) is linear in $\Upsilon^{n,m}$ and, while these equations are coupled, the form of the S^{nm} allows these equations to be solved sequentially; each equation in the sequence depending only, through S^{nm}, on the previously computed solutions. Specifically, the system can be solved explicitly in the order $\Upsilon^{0,m}$, $m = 0, \ldots, M$; $\Upsilon^{1,m}$, $m = 0, \ldots, M-1$; $\Upsilon^{2,m}$, $m = 0, \ldots, M-2$ *etc*.

NUMERICAL METHOD

The conservative and linear convection-diffusion equations defined by Eqn. (15) exhibit specific features that complicate the construction of a numerical scheme. For example the coefficients $v_2, \mathcal{F}_2, \mathcal{G}_2$ vary over the range $\langle -\infty, \infty\rangle$ so that convection or diffusion dominates in different parts of the domain. Secondly, diffusion is only present in the fluid velocity dimension. Furthermore, solutions to Eqn. (15) typically vary from smooth near-Gaussian distributions to highly peaked profiles near the wall where the turbulence is small, in particular with respect to the dimensions corresponding to the normal components of particle velocity and position. It is these characteristics that motivate the use of (nodal) Discontinuous Galerkin methods [12] being flexible and able to handle convection dominated systems to represent the solution in (x_2, v_2)-space. With respect to the fluid velocity dimension the solution is often strongly localised near a surface in phase space, in particular when the particle response time $\tau_p = \beta^{-1} \not\gg 1$. For spatially invariant systems, for example, this surface is given by the plane $u_2 = (v_2 - v_{g2})/\sigma_2$. Therefore, the fluid velocity dimension is mapped such that $\tilde{\Upsilon}^{n,m}$ is localised around $\tilde{u}_2 = 0$, and has unit variance,

$$\tilde{u}_2 = \frac{u_2 - u_0(x_2, v_2)}{\sigma_u(x_2, v_2)}. \quad (17)$$

It is anticipated that $\tilde{\Upsilon}^{n,m}$ remains near-Gaussian in the scaled fluid velocity dimension $\tilde{u}_2$, also close to the wall. Therefore, a Hermite spectral method is used, see [4]. This results in a system of N_u coupled linear convection equations.

The computational domain is further defined in terms of the scaled coordinates

$$(\tilde{x}_2, \tilde{v}_2) = \left(\frac{2x_2 - (X + X_0)}{X - X_0}, \frac{v_2}{\sigma_{p2}}\right), \quad (18)$$

to map (x_2, v_2)-space to a standard rectangle. $\sigma_{p2} = \sigma_2\sqrt{\eta_2}$ represents the approximate particle velocity RMS at $x_2 = X$ as in Eqn. (9). This domain is divided in an unstructured triangular mesh of M elements, generated using the freely available DistMesh software, [13]. The also freely available Matlab implementation of the two-dimensional nodal DG method, [12], is, in adapted form, used to construct linear algebraic equations for $\hat{\tilde{\boldsymbol{\Upsilon}}}^{n,m}$ of the form

$$(\boldsymbol{A}_0 + \boldsymbol{A}_{n,m})\cdot\hat{\tilde{\boldsymbol{\Upsilon}}}^{n,m} = \boldsymbol{b}_{\mathrm{bc}}^{n,m} + \hat{\tilde{\boldsymbol{\mathcal{S}}}}^{n,m}, \quad (19)$$

in which, for efficiency reasons, the global matrix is decomposed in a (n,m)-specific diagonal matrix $\boldsymbol{A}_{m,n}$ and in matrix $\boldsymbol{A}_0$, that is independent of n, m and, hence, has to be constructed only once. The conditioned moments, $\hat{\tilde{\boldsymbol{\Upsilon}}}^{n,m}$, are now calculated sequentially for all n, m of interest, starting with $\hat{\tilde{\boldsymbol{\Upsilon}}}^{0,0}$. The matrix is for the configurations considered here sufficiently sparse and banded to allow direct matrix inversion.

What remains is the specification of the coefficients $u_0(x_2, v_2)$ and $\sigma_u(x_2, v_2)$ in Eqn. (17). Ideally they would be defined as the conditional mean and RMS of $\Upsilon^{0,0}$, with respect to dimension u_2 and for given v_2, so

$$u_0 = \frac{1}{p}\int u_2 \Upsilon^{0,0}\mathrm{d}u_2, \quad \sigma_u^2 = \frac{1}{p}\int (u_2 - u_0)^2 \Upsilon^{0,0}\mathrm{d}u_2, \quad p = \int \Upsilon^{0,0}\mathrm{d}u_2. \quad (20)$$

If the configuration is relatively simple, e.g. when the turbulence is taken homogeneous throughout the full domain, or when the particles are heavy, $\tau_p = \beta^{-1} \gg 1$, then the specific relation for

the coefficients may be based on the spatially invariant distribution $\phi(v_2, u_2)$. In this case the coefficients (20) are given by

$$u_0 = \frac{v_2 - v_{g2}}{\sigma_2}, \quad \sigma_u = \sqrt{\frac{\tau_p}{\tau_p + \tau_2}}. \tag{21}$$

For more complicated systems the scaling coefficients are calculated iteratively. In each iteration the system is slightly changed by increasing the 'degree of turbulence inhomogeneity', represented by fluid weight $0 < w_f < 1$. That is the adopted fluid statistics, $\widetilde{\langle \boldsymbol{U}'\boldsymbol{U}' \rangle}$, $\widetilde{\tau_f}$, are defined as the weighted mean of the original fluid statistics and their value at $x_2 = X$,

$$\widetilde{\langle \boldsymbol{U}'\boldsymbol{U}' \rangle}|_{x_2} = w_f \langle \boldsymbol{U}'\boldsymbol{U}' \rangle|_{x_2} + (1 - w_f)\langle \boldsymbol{U}'\boldsymbol{U}' \rangle|_X, \tag{22}$$

$$\widetilde{\tau_f}(x_2) = w_f \tau_f(x_2) + (1 - w_f)\tau_f(X). \tag{23}$$

For example, zero fluid weight implies homogeneous turbulence in the entire domain, whereas $w_f = 1$ means the real fluid statistics. The scaling parameters for the next iteration are redefined based on the current solution $\hat{\tilde{\boldsymbol{\Upsilon}}}^{0,0}$, starting with $w_f = 0$.

In practise, however, calculating the scaling coefficients $u_0(x_2, v_2)$, $\sigma_u(x_2, v_2)$ as in (20) is in parts of the domain too strongly affected by numerical noise, for example when $\Upsilon^{0,0} \to 0$, or by small overshoots near under-resolved gradients in the solution. Therefore a least-squares approach is employed: u_0, σ_{u_2} are approximated by continuous piecewise polynomial basis that is linear in each element. To find the associated coefficients we define for all MN_{xv} nodes i in the $(\tilde{x}_2, \tilde{v}_2)$-plane the integrals

$$\hat{p}_i = \int \Upsilon_i^{0,0} \mathrm{d}u_2, \quad \widehat{pu}_i = \int u_2 \Upsilon_i^{0,0} \mathrm{d}u_2,$$

$$\widehat{puu}_i = \int u_2^2 \Upsilon_i^{0,0} \mathrm{d}u_2, \tag{24}$$

and discard all three if, for given i, $\hat{p}_i$ is smaller than a certain threshold, $\hat{p}_i < p_c$ (typically $p_c = 10^{-2}$). In addition, it is required that the ratio of the N_u^{th} and the 1^{st} coefficient of the Hermite functions at node i be smaller than $1/N_u^2$. The discarded values $\hat{p}_i$, $\widehat{pu}_i$, $\widehat{puu}_i$ are replaced by, respectively, p_c, $p_c\tilde{u}_0$, $p_c(\tilde{\sigma}_u^2 + \tilde{u}_0^2)$, with $\tilde{u}_0$, $\tilde{\sigma}_u$ approximations in the previous iteration. Let L_{ij} be the j^{th} basis function evaluated at node i. Then the associated coefficients $c_{u,j}$, $c_{\sigma,j}$ are specified by the least squares solutions to, respectively,

$$\sum_j \hat{p}_i L_{ij} c_{u,j} = \widehat{pu}_i, \tag{25}$$

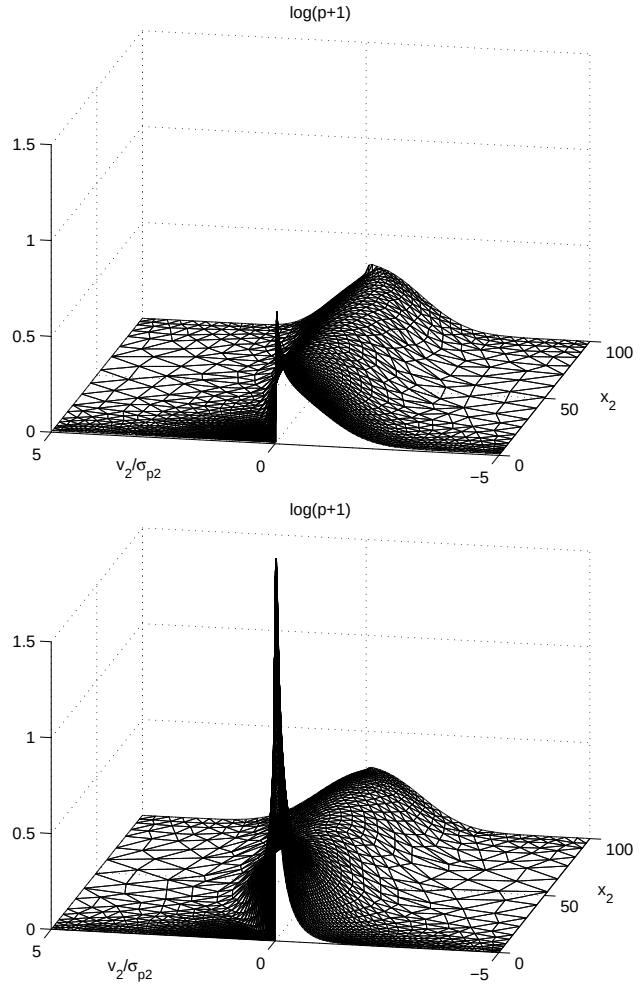

FIGURE 2. PDF FOR: $\tau_p = 300$ (TOP), $\tau_p = 10$ (BOTTOM).

and

$$\sum_j \hat{p}_i^2 L_{ij} c_{\sigma,j} = \hat{p}_i \left(\widehat{puu}_i - \widehat{pu}_i^2 \right). \tag{26}$$

Estimates of the scaling coefficients at node i are then given by

$$u_{0,i} = \sum_j L_{ij} c_{u,j}, \quad \sigma_{u,i}^2 = \max \left[\sum_j L_{ij} c_{\sigma,j}, 10^{-3} \right]. \tag{27}$$

RESULTS

We consider the boundary configuration as sketched in Fig. 1. The value for the boundary layer thickness, in wall units, is set to $X = 100$. Following [11], [14] we take $\rho_p/\rho_f = 770$.

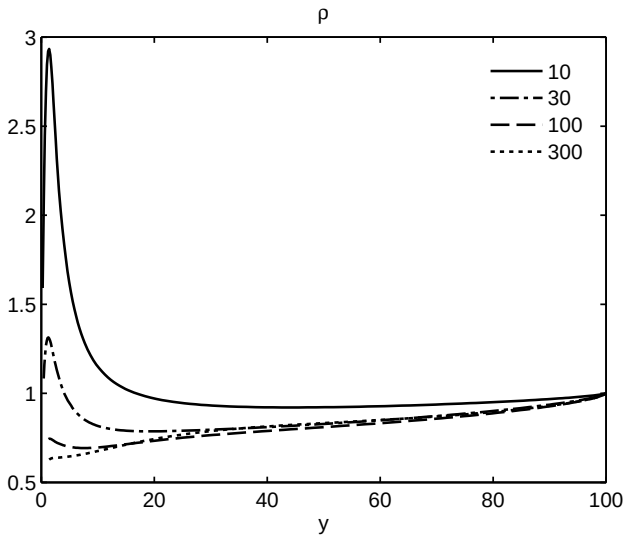

FIGURE 3. PARTICLE CONCENTRATION IN THE BOUNDARY LAYER FOR DIFFERENT τ_p.

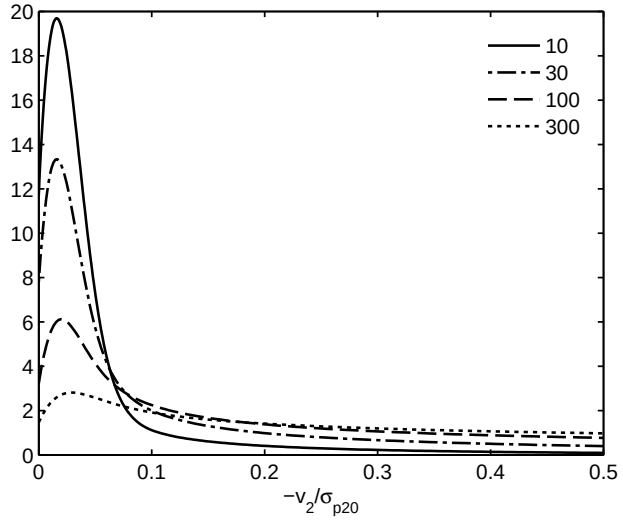

FIGURE 4. NORMALISED VELOCITY DISTRIBUTION AT THE WALL ($x_2 = X_0$) FOR DIFFERENT τ_p.

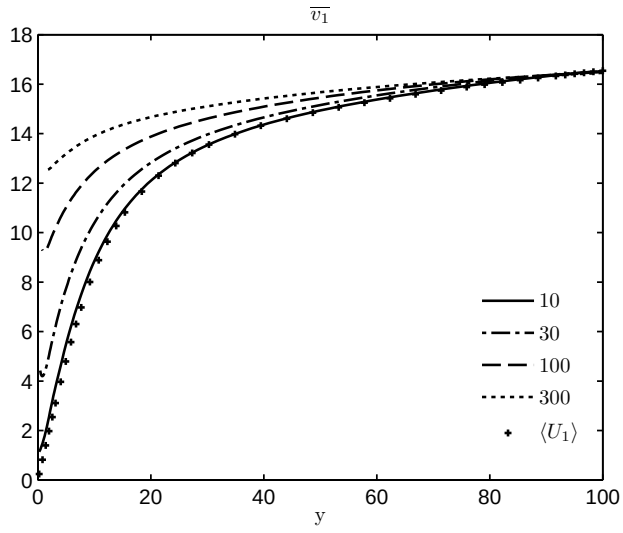

FIGURE 5. STREAMWISE PARTICLE VELOCITY IN THE BOUNDARY LAYER FOR DIFFERENT τ_p.

The calculations have been carried out using fourth order elements and 8 Hermite functions. The solution $\Upsilon^{0,0}$ is calculated in 10 iterations in which the fluid weight, see Eqn. (22), is increased from $w_f = 0$ to $w_f = 0.999$. The reason for limiting the fluid weight (not setting $w_f = 1$) is to moderate the sharp peak near the wall slightly, see Fig. 2. Then less elements are required to represent the solution such that direct matrix inversion is still feasible without compromising the characteristics of the solution too much. The numerical method has been assessed by grid refining, and by comparing the moments of various solutions to the associated random walk simulation. The results were close to identical, as they should be. Probably the best test for the numerics is to verify whether the particle current, $\rho\overline{v_2}$, is constant throughout the boundary layer. The maximum deviation from the spatially averaged current was observed for $\tau_p = 10$ and was less than 1% of the mean current. It is noted that all variables are expressed in wall units.

Figure 2 presents the equilibrium particle pdfs corresponding to two different values of τ_p. Since the range of the pdf is too large for clear visualisation the quantity $\log(p+1)$ is presented instead of p itself. The figure shows that particles enter the domain at $x_2 = 100$ for $v_2 < 0$, and subsequently move towards the wall via, mainly, a diffusive mechanism. Closer to the wall, at about $x_2 = 20$, the fluid RMS decreases rapidly.

The effect is that the particles cannot follow the close-to-equilibrium state and start moving in free flight. Most of the heavy particles ($\tau_p = 300$, see Fig. 2 (top)) have enough momentum to reach the wall, even the ones that have a relatively low speed. Only very slow particles get trapped near the wall, and slowly drift towards absorption at $x_2 = X_0$. This results in a small build-up of particles near the wall at low velocity. For lighter particles ($\tau_p = 10$, see Fig. 2 (bottom)) only the fast particles reach the wall in free flight while most will be trapped. This results in a strong build-up which is also clearly visible in Fig. 3, where the particle concentration in the boundary layer is shown. In the figure the small build-up of heavy particles is not visible because their weight is too low to contribute significantly to the averages. The normalised particle velocity distribution at $x_2 = X_0$, presented in Fig. 4, illustrates this process as well. That the concentration peaks just off the wall is quali-

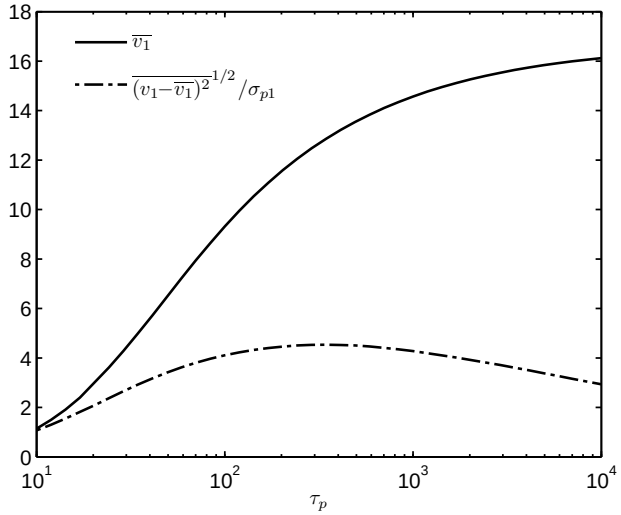

FIGURE 6. STREAMWISE PARTICLE VELOCITY AND RMS AT THE WALL ($x_2 = X_0$) AGAINST τ_p.

tatively in agreement with DNS data, [15], although in the paper this effect occurs at much smaller τ_p. Also, [15] report a concentration build-up that is larger than that in Fig. 3 for small particles; values of $\tau_p > 25$ have not been considered in the paper. It is expected that agreement is better when the fluid weight is $w_f = 1$.

The streamwise particle velocity $\overline{v_1}$ in the boundary layer is visualised in Fig. 5. Small particles follow the mean fluid velocity, $\langle U_1 \rangle$, well. Since their normal velocity v_2 is very low near the wall there is enough time to accommodate to the fluid velocity. Heavy particles, in contrast, cross the near wall region quickly and maintain their streamwise momentum, see also Fig. 6. It can also be observed in Fig. 6 that the model predicts a strong increase of the streamwise velocity RMS at $x_2 = X_0$ compared to σ_{p1}. The same effect can be viewed in Fig. 7 (top). It is noted that the normal component of the particle velocity RMS, Fig. 7 (middle), is smaller than one at $x_2 = X$, in particular for large τ_p. This due to the boundary condition at $x_2 = X$. For small particles the influence of the wall on the pdf is small at $x_2 = X$, since their mean free path is much smaller than $X = 100$. This is not true for large particles. Therefore the imposed velocity distribution at $x_2 = X$, Eqn. (8), is unlikely to be fully consistent with the distribution that one would expect when the domain had not been truncated but coupled to the core of the flow for $x_2 > X$. Consequently σ_{p2} overestimates the normal component of the particle velocity RMS.

DISCUSSION

A Hermite-Discontinuous Galerkin scheme is has been presented to treat a system of coupled fluid-particle pdf equations

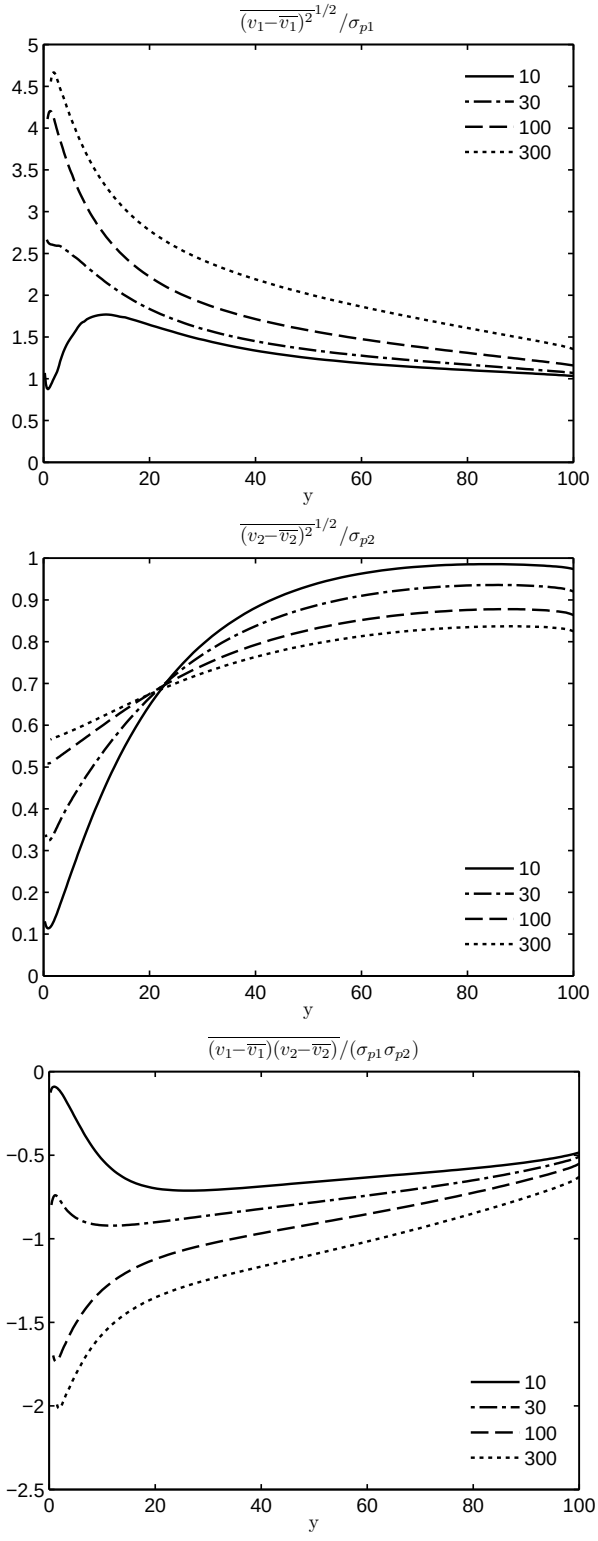

FIGURE 7. PARTICLE VELOCITY RMS' AND PARTICLE KINETIC STRESS FOR DIFFERENT τ_p.

to describe the transport of phase-space conditioned moments of particle and fluid velocities, both streamwise and wall-normal. The choice of Hermite basis functions and an iterative rescaling approach, allow for efficient discretization of the, effectively, 5-dimensional phase-space domain. Examples have shown the effectiveness of both the numerical scheme and the phase-space transport equations. The method provides a computationally efficient way to study particle transport in boundary layers. The method produces smooth solutions compared to the associated random walk simulation. This facilitates numerical differentiation of the pdf, a useful property for constructing closure relations for transport equations for mass, momentum, and kinetic stress.

Future development of the methodology include different boundary conditions, such as partially absorbing walls, and rough walls, and effects of gravity.

ACKNOWLEDGMENT

The authors gratefully acknowledge the financial support of this work by the UK Engineering and Physical Sciences Research Council, EP/D061601.

REFERENCES

[1] Reeks, M., 1991. "On a kinetic equation for the transport of particles in turbulent flows". *Phys. Fluids,* ***3***, pp. 446–456.

[2] Buyevich, Y., 1971. "Statistical hydrodynamics of disperse systems. Part 1: Physical background and general equations". *J. Fluid Mech.,* ***49***, pp. 489–507.

[3] Simonin, O., Deutsch, E., and Minier, J., 1993. "Eulerian prediction of the fluid/particle correlated motion in turbulent two-phase flow". *Appl. Sci. Res.,* ***51***, pp. 275–283.

[4] Swailes, D., and Reeks, M., 1994. "Particle deposition from a turbulent flow. I: A steady-state model for high-inertia particles". *Phys. Fluids,* ***6***, pp. 3392–3403.

[5] Aguinaga, S., Simonin, O., Borée, J., and Herbert, V., 2009. "A simplified particle-turbulence interaction model: Application to deposition modelling in turbulent boundary layer". In ASME 2009 Fluids Eng. Div. Summer Meeting FEDSM2009, Vail, Colorado USA.

[6] Iliopoulos, I., and Hanratty, T., 2004. "A non-Gaussian stochastic model to describe passive tracer dispersion and its comparison to a direct numerical simulation". *Phys. Fluids,* ***16***, pp. 3006–3030.

[7] Mito, Y., and Hanratty, T., 2002. "Use of a modified langevin equation to describe turbulent dispersion of fluid particles in a channel flow". *Flow, Turb. and Comb.,* ***68***, pp. 1–26.

[8] Thomson, D., 1987. "Criteria for the selection of stochastic models of particle trajectories in turbulent flows". *J. Fluid Mech.,* ***180***, pp. 529–556.

[9] Risken, H., 1996. *The Fokker-Planck Equation*, 2^{nd} ed. Springer-Verlag, Berlin.

[10] Kim, J., Moin, P., and Moser, R., 1987. "Turbulence statistics in fully developed channel flow at low Reynolds number". *J. Fluid Mech.,* ***177***, pp. 133–166.

[11] Kallio, G., and Reeks, M., 1989. "A numerical simulation of particle deposition in turbulent boundary layers". *Int. J. Multiphase Flow,* ***15***, pp. 433–446.

[12] Hesthaven, J., and Warburton, T., 2008. *Nodal Discontinuous Galerkin Methods*. Springer.

[13] Persson, P., and Strang, G. "A simple mesh generator in Matlab". *SIAM Review,* ***46***.

[14] Liu, B., and Agarwal, J., 1974. "Experimental observation of aerosol deposition in turbulent flow". *Aer. Sci.,* ***5***, pp. 145–155.

[15] Marchioli, C., Soldati, A., Kuerten, J., Arcen, B., Tanière, A., Goldensoph, G., Squires, K., Cargnelutti, M., and Portela, L., 2008. "Statistics of particle dispersion in direct numerical simulations of wall-bounded turbulence: Results of an international collaborative benchmark test.". *Int. J. Multiphase Flow,* ***34***, pp. 879–893.